

This version of the article has been accepted for publication, after peer review (when applicable) and is subject to Springer Nature's AM terms of use, but is not the Version of Record and does not reflect post-acceptance improvements, or any corrections. The Version of Record is available online at:
<https://doi.org/10.1007/s40430-022-03368-3>

Investigation on the flexural properties of sandwich beams with auxetic core

Milad Najafi¹, Hamed Ahmadi^{1*}, GholamHossein Liaghat^{1,2}

¹ Faculty of Mechanical Engineering, Tarbiat Modares University, Tehran, Iran.

² School of Mechanical & Aerospace Engineering, Kingston University, London, United Kingdom.

(*corresponding author: Hamed Ahmadi, Faculty of Mechanical Engineering, Tarbiat Modares University, Jalal Highway, Tehran, Iran. Email: h_ahmadi@modares.ac.ir)

Abstract

Availing cellular structures as the core of sandwich beams is an innovative approach to improve the efficiency of them. Nonetheless, the flexural characteristics of sandwich beams is affiliated to the core topology. Accordingly, choosing an appropriate core can have a significant efficacy on the performance of sandwich beams. The purpose of the present study is to assess the influence of using auxetic cores in flexural properties of sandwich beams. Specifically, experimental and finite elements approaches were implemented to evaluate the flexural behavior, energy absorption and the stiffness of fully integrated 3D printed polymeric sandwich beams, made of ‘square node anti-tetra chiral, arrowhead and re-entrant auxetic cores was investigated and compared with the conventional honeycomb core. Fabrication of specimens was performed using FDM 3D printing method and three point bending tests were conducted on the printed specimens. Results indicated that selection of proper core topology has remarkable effect on the flexural properties of sandwich beams, and using auxetic core is potentially an efficient method to enhance mechanical properties of sandwich beams duo to high load bearing capacity.

Keywords: Sandwich beams; Auxetic core; Flexural behavior; Three-point bending test; FDM 3D printing method.

1. Introduction

There is a growing interest in using lattice cores to design sandwich structures because of their reduced weight and enhanced mechanical properties. One of the oldest and most widely used of these structures is the honeycomb core sandwich structure that designed and inspired by nature [1–3]. Currently, cellular materials are also used as core of sandwich composites [4]. The cellular architecture determines the mechanical behavior and can affect a wide range of properties, e.g., acoustic, thermal, and biological properties [5]. Using lightweight sandwich structures with proper

core topology have many advantages such as high stiffness-to-weight ratio and high energy absorption capability [6]. Conventional methods used to manufacture the sandwich structures have many limitations for the structures with different geometries [7], while, the additive manufacturing (AM) is the state-of-the-art technology that changed the conventional approach to manufacturing systems [8]. 3D printing is an additive manufacturing technique widely used in the automotive and civil construction systems to obtain lightweight sandwich structures made with complex core shapes to achieve excellent multifunctional properties, such as flexural stiffness, and high energy-absorption capabilities [9]. The complex geometries and structures which otherwise are difficult to achieve by using traditional methods can be performed with the help of Fused Deposition Modeling (FDM) 3D printing method [10].

Materials and structures with negative Poisson's ratio exhibit a counter-intuitive behaviour. Under uniaxial compression (tension), these materials and structures contract (expand) transversely. The materials and structures that possess this feature are also termed as 'auxetics' [11]. Auxetic metamaterials are synthetic materials with microstructures engineered to achieve negative Poisson's ratios. The auxetic structures are the frames that fabricated from non-auxetic materials, but show auxetic behavior in overall. Lakes first presented a re-entrant foam with NPR in 1987 [12], since then, many researchers have introduced various structures based on geometrical techniques to exhibit auxetic behavior, such as arrowhead structure, chiral structures, etc. [13–15]. On the other hand, auxetic metamaterials has been attracted special attention in recent years because of their unusual properties and many potential applications in various fields [12] including vibroacoustic applications [16–18], indentation resistance, fracture toughness, variable permeability, energy absorption [11,19,20] and other engineering fields such as packaging, biomedicine, sensors, automotive engineering, etc. [13, 21].

Ingrole et al. [22] investigated the energy absorption of re-entrant auxetic structure and performed a modification on its geometry and compared with the non-auxetic honeycomb structure in terms of energy absorption and other mechanical properties and found that auxetic structures have a better energy absorption performance. Chang et al. [23] also with experimental and numerical investigation of the re-entrant structure and the honeycomb, found that the performance of the re-entrant auxetic structure in absorbing the energy of impact and close in blast loading is better than the honeycomb structure. Safikhani Nasim and Etemadi [24] discovered a new model of auxetic structures in the form of warp and woof re-entrant auxetic structure. Yazdani Sarvestani et al. [6] compared failure mechanism, energy absorption and multi hit capability of 3D printed meta sandwich structures. Castro et al. [9] investigated mechanical behavior of three types of 3D printed polymer sandwich structures in tensile, flexural and Charpy impact tests. Šubic et al. [25] investigated mechanical characteristics of slender hybrid wood-based beams in terms of bending

stiffness, load bearing capacity and flexural rigidity. Zaharia et al. [10] evaluated the mechanical performance of additively manufactured lightweight sandwich structures with honeycomb, diamond-celled and corrugated core shapes. Spahic et al. [4] performed a multi-scale analysis on the flexural behaviour of 3D printed cellular polymer materials for comparison between morphing and sandwich beams. Hou et al. [26] presented a comparative study on the reliability of auxetic and non-auxetic lattice composites and found that the panel with re-entrant core performs best in both force mitigation and energy dissipation, provided that the impact energy is appropriate. Sadeghian et al. [27] studied the flexural behavior of sandwich composite beams made of fiber reinforced polymer (FRP) skins and light-weight cores. Gebrehiwot et al. [8] assessed the flexural behavior of 3D printed polylactic acid (PLA) beams with five types of stiffener geometries.

Based on the literature, it can be deduced that sandwich structures with cellular cores have many potentials, although in recent years, various studies have been conducted to investigate the mechanical characteristics of sandwich structures with different cores, nevertheless less attention has been paid to investigate the influence of using auxetic cores on the flexural properties, load bearing capacity and energy absorption capability of additively manufactured beams.

Present research, assessed the structural response, stiffness and energy absorption capability of fully integrated 3D printed sandwich beams. The effect of core topology on the flexural properties of lightweight sandwich beams is studied to properly select and design the microstructure of sandwich beams to attain desirable structural requirements. Three types of different auxetic core topologies including re-entrant, square node anti-tetra chiral and arrowhead, are considered for sandwich beams and compared with non-auxetic honeycomb core sandwich beam. Finite element simulation and experimental testing were implemented to evaluate the flexural behavior of sandwich beams. Fused deposition modeling (FDM) additive manufacturing method was used to fabricate the specimens and three-point bending test conducted on the specimens to find their flexural characteristics. Moreover, failure mechanisms during deflection of the beams are investigated.

2. Materials and methods

2.1 fabrication of specimens

2.1.1 Topology of structures

In the present work, sandwich beams with four different core topologies have been studied. Fig. 1 represents the unit cells of honeycomb, re-entrant, arrowhead and anti-tetra chiral structures, respectively. In the previous work [20], authors used these patterns for investigation of energy absorption of sandwich structures in quasi static compression and low velocity impact loading.

The single most important feature of a cellular solid is its relative density, ρ^* / ρ_s [28]; that is density of cellular solid, ρ^* , divided by the density of bulk material (in this work, acrylonitrile butadiene styrene (ABS)), ρ_s . Relative density values for different beams are calculated and given in Table 1.

Design parameters for each unit cell are shown in Fig. 1 and Table 1. Design parameters of unit cells are as follows: in honeycomb and re-entrant unit cells, h and l denote the length of vertical and inclined cell walls respectively, while α is the angle of inclined walls. For the square node anti-tetra chiral, h and l denote the length of vertical and horizontal cell walls respectively, while a is the length of the side of square in the square node anti-tetra chiral unit cell. Finally, for the arrowhead unit cell, h and l denote the length of longer and shorter inclined cell walls respectively, while α is the angle of shorter inclined walls. Moreover, t is the thickness of cell walls in all unit cells. The number of unit cells and total dimensions of structures in height, width and depth were approximately identical to make comparable designs.

Table 1. Dimension of unit cells of each model

Structure	$h(mm)$	$l(mm)$	$a(mm)$	$t(mm)$	$\alpha(^{\circ})$	<i>Relative density</i>
Re-entrant	10	5	-	1	30	0.3517
Arrowhead	13.50	8.40	-	1	30	0.4015
Anti-tetra chiral	9.80	9.80	2	1	-	0.3643
Honeycomb	5.20	5.20	-	1	30	0.2758

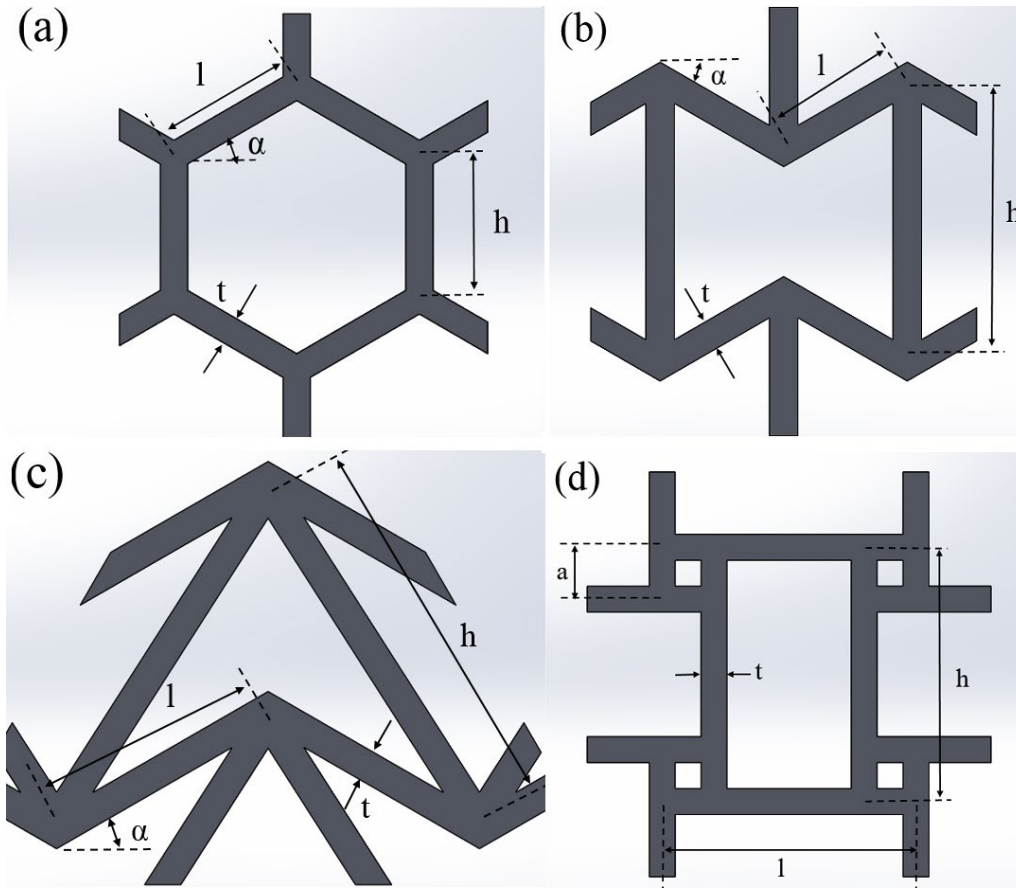


Fig. 1. Design of unit cells: (a) honeycomb, (b) re-entrant, (c) arrowhead, (d) square node anti-tetra chiral

2.1.2 The process of fabrication

Four different models were created using the design parameters mentioned in Table 1. The depth of the specimens was considered equal to their thickness, 30 mm. For each model, three samples have been manufactured and tested. Fig. 2 shows specimens fabricated using additive manufacturing. Fabrication of specimens was conducted using fused deposition modeling (FDM) process. The sandwich beam models are fabricated using QUANTOM 3D printing machine. The printing parameters of the specimens are given in Table 2. The purpose of selecting these parameters for printing specimens was to have samples with the shortest possible time for printing, while having smooth surfaces without geometric defects. The required time for printing of tensile specimens was about 30 minutes and for beam specimens, varied from about 6 hours up to 9 hours. A filament with 1.75 mm diameter was used. It should be noted that the manufacturing direction of specimens was z-direction.

Table 2. Printing parameters used to fabrication of specimens

Layer Height	Nozzle Temp.	Bed Temp.	Infill Percentag e	Cooling	Nozzle Diameter	Extrusion Width
0.2 mm	243 ± 5	85 ± 5	100 %	OFF	0.4mm	0.51 mm

At the top and bottom of all structures, two face sheets were designed with 1 mm thickness. This face sheets which are skins of the sandwich beams, act as continuous surfaces for the rollers to ensure that the loads are applied efficiently for the three point bending tests [4]. The base material used to fabricate the test specimens was ABS (acrylonitrile butadiene styrene). In order to assess the properties of the base material, five tensile test specimens were fabricated and tested according to ASTM-D638 standard.

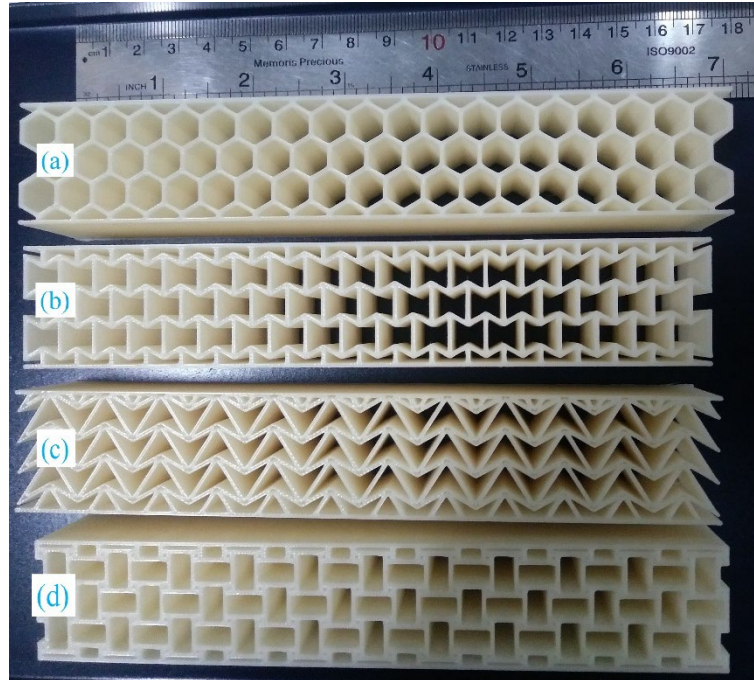


Fig. 2. Fabricated specimens: (a) honeycomb, (b) re-entrant, (c) arrowhead, (d) anti-tetra chiral

Fig. 3 shows the fabricated dumbbell-shaped specimen subjected to the tensile loading. True stress-strain curve of ABS material presented in Fig. 4 and its average mechanical properties of tests data that are mentioned in Table 3. Mechanical properties of dumbbell-shaped test specimens (average of 5 test specimens), are used to define material properties in finite element simulation.

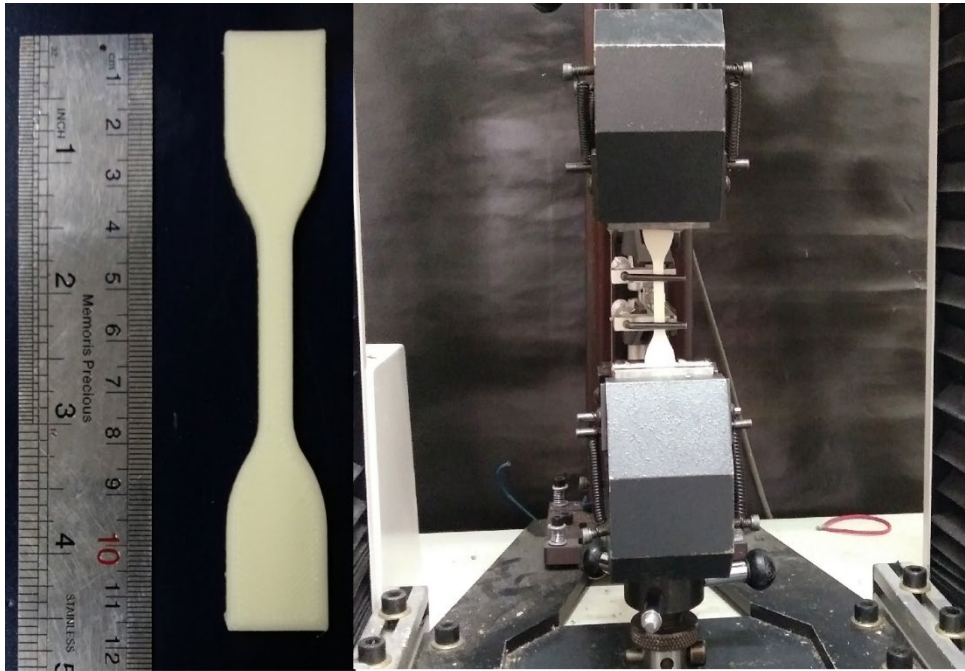


Fig. 3. 3D-printed dumbbell-shaped specimen subjected to uniaxial tensile loading according to ASTM-D638

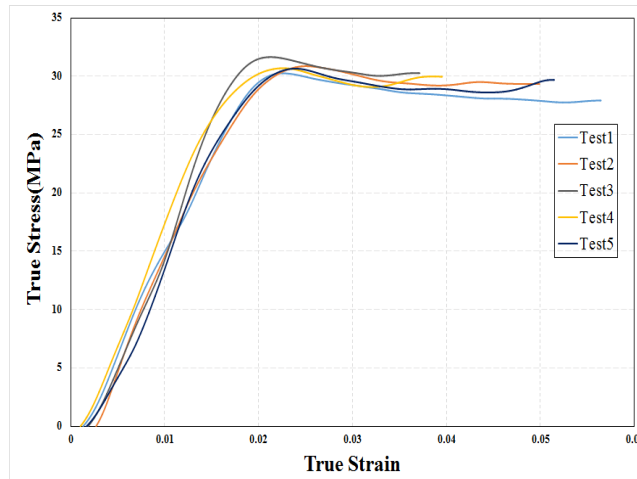


Fig. 4. True stress-strain curve of dumbbell-shaped test specimens

Table 3. Mechanical properties of dumbbell-shaped test specimens (average of 5 test specimens)

Base material	Young's modulus (MPa)	0.2% offset yield stress (MPa)	Poisson's ratio [22]	Density(g/cm ³)
ABS	1900 ± 10	30 ± 1	0.35	0.94 ± 0.03

Table 4. Defined plastic properties in finite element simulation based on true stress-strain curve data

Plastic strain	0	0.003	0.007	0.012	0.016	0.020	0.024
Plastic stress (MPa)	29.25	30.39	30.00	29.47	29.10	28.75	28.31

2.2 Test setup

As shown in Fig. 5, the in-plane three-point bending tests of manufactured specimens were performed using a universal servo-hydraulic testing machine at the crosshead speed of 2 mm/min. Due to the design and experimental testing facilities limitations, such as geometrical restrictions of flexural test machine, the tests were performed in according with the ASTM-C393 standard, as much as feasible. Considering the equal number of cells in all of the sandwich beams, the approximate length of the beams was considered to be 170 ± 5 mm. The span length of testing was set on 120 mm and the span to thickness ratio (L_s) of four 3D printed specimens 4. Furthermore, depth of the samples was 30 mm, which was equal to their thickness. The load was applied by cylindrical central roller with 15 mm diameter and two support rollers used with the same diameter. The output of testing machine were force-displacement values that were recorded for further analysis.

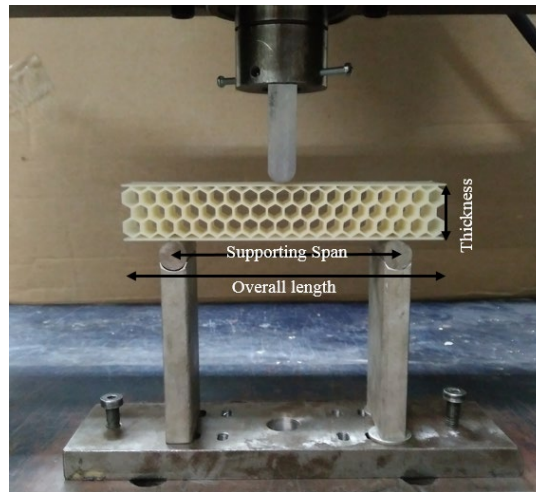


Fig. 5. Quasi-static three-point bending testing setup

3. Finite Element Simulation

Finite element analysis was carried out using ABAQUS CAE package to simulate the behavior of sandwich beams under three point bending tests. Explicit models were constructed by solid elements and the depth of beams was 30 mm. Dimensions of the models were the same as mentioned in Table 1 and Section 2.2. The average tensile test results of dumbbell-shaped specimens were used to define the material properties. The true stress-strain curve was obtained from the nominal

stress-strain curve's data, and used for definition of the material properties in FEM modeling which are given in Table 3 and Table 4. The complete model of structures is shown in Fig. 6.

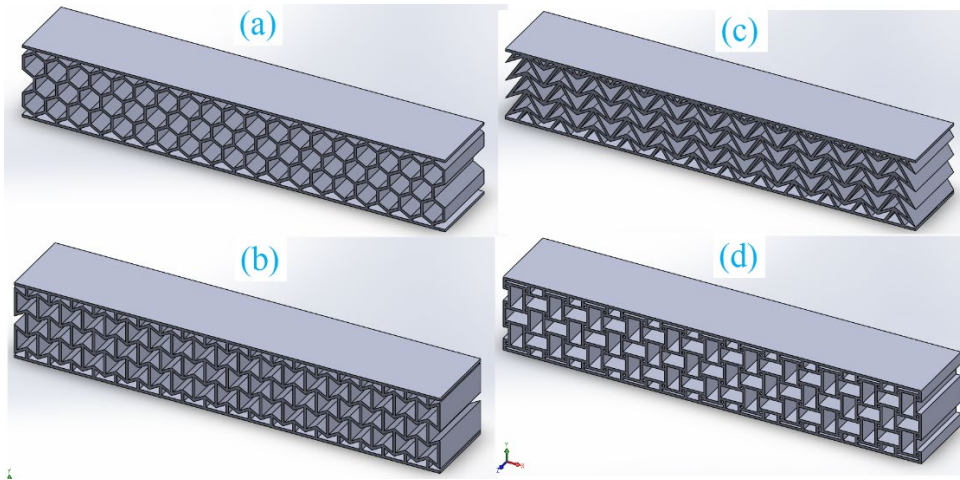


Fig. 6. Complete form of beams: (a) honeycomb, (b) re-entrant, (c) arrowhead, (d) square node anti-tetra chiral

Sandwich beams under a quasi-static three-point bending load were simulated as shown in Fig. 7. Meshing of the models was performed using linear 8-node solid elements with reduced integration (C3D8R) and the mesh was sweep with hexahedral elements. To simulate the experimental tests, the model was placed on two cylindrical rollers and another roller applied downward displacement on the specimen. The cylindrical rollers were simulated as rigid bodies with a reference point at the center. A general contact algorithm was applied for the interaction property that was defined as ALL WITH SELF with a normal behavior and a tangential behavior with the friction coefficient of 0.2. For the quasi-static three-point bending, a downward displacement load was applied on the top roller in y-direction and the other degrees of freedom were fixed and the supporting rollers are fixed for all degrees of freedom.

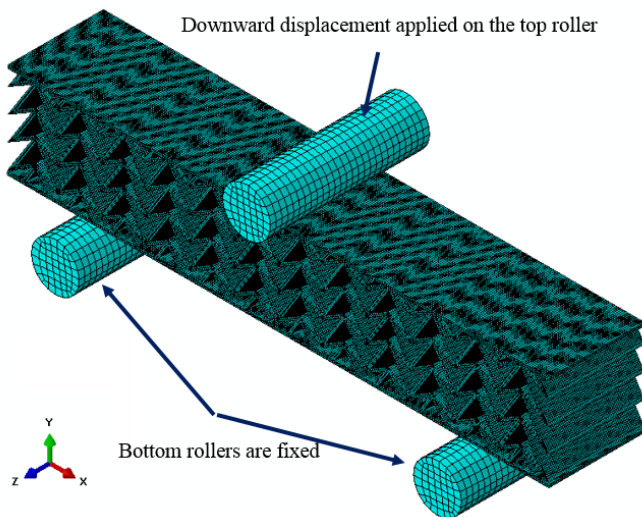


Fig. 7. Finite element model for three-point bending test

To assign appropriate element size and avoiding mesh dependency of FEM results, three size of elements including 1 mm, 0.5 mm and 0.25 mm were utilized for meshing of the honeycomb core sandwich beam as an example. The load-deformation curves of this element sizes are shown in Fig. 8. The FEA results of 0.5mm and 0.25 mm element sizes were similar, indicating converged solution. Consequently, to reduce the numerical analysis time, the current FE models were created using element size of 0.5 mm.

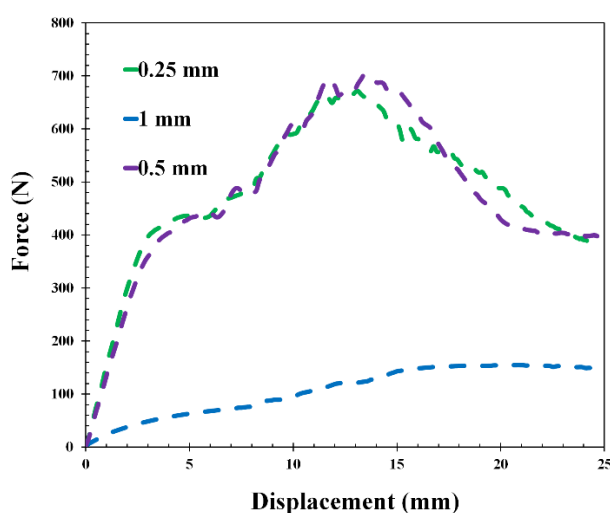


Fig. 8. Mesh convergence curves of honeycomb sandwich beam using different element sizes

4. Results and Discussion

Quasi-static three-point bending tests were conducted on fabricated specimens using a universal testing machine at the crosshead speed of 2 mm/min. Fig. 9 presents and compares the experimental and numerical force-displacement curves of 3D printed sandwich beams under three-point bending load. The behavior of the specimens, under compression loading in y-direction, was recorded step by step, so that the deformation behavior and structural performance of the structures, could be analyzed during displacement-controlled tests. Fig. 10 shows the detail deformation pattern and collapse behavior of the specimens. As it can be seen from Fig. 10, for the sandwich beams with auxetic cores, under the loading location, the localized aggregation of unit cells occurs and all the unit cells of the structure are inclined toward the center of the beam. Having negative Poisson's ratio is the reason of this phenomenon. Due to the unit cell concentration under the loading location, the load bearing capacity of these structures are higher than that of non-auxetic honeycomb sandwich beam. Fig. 9 presents a comparison of the force-displacement curves of 3D printed sandwich beams with re-entrant, arrowhead and square node anti-tetra chiral geometries and non-auxetic honeycomb core sandwich beam obtained by the results of experimental tests and numerical

simulations. There is a good agreement between the experimental and numerical results to the displacement range where the first failure occurs in the cell wall of the structures. After the first failure in the wall of the unit cell, the experimental and numerical results are inconsistent, because the elastic-plastic model is used to define the material properties in finite element simulations and no failure criteria is defined. When the displacement exceeds a certain range, the failure of the unit cell wall causes a sudden drop in the amount of force which is not predicted by the finite element model.

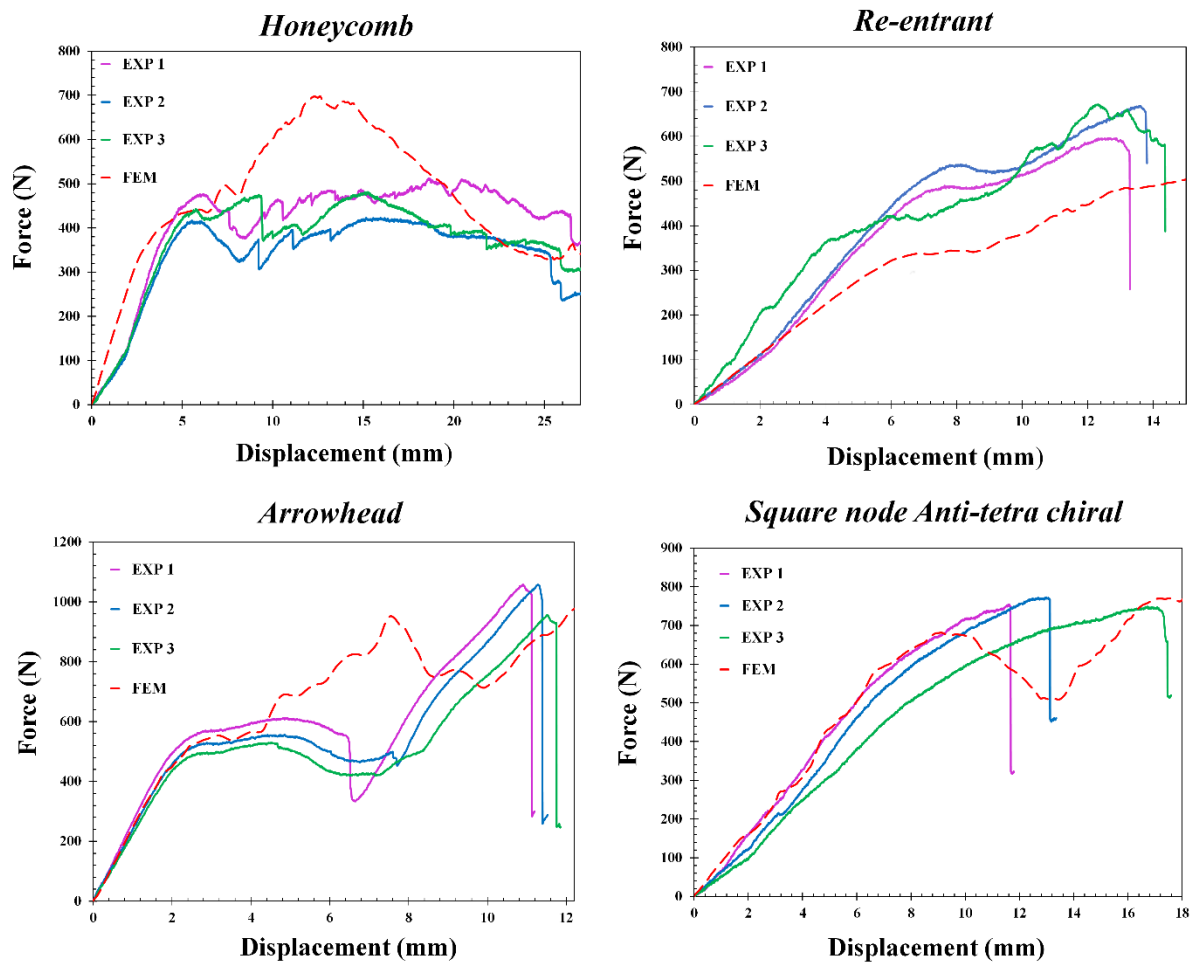


Fig. 9. Force-displacement curves for sandwich beams

Fig. 10 shows corresponding deformed configurations in the experimental tests and FEA simulations (Von Mises stress distributions) of sandwich beams. Table 5 presents the maximum loads and flexural stiffness of sandwich beams obtained by experimental tests and numerical analysis. The flexural stiffness values are obtained by calculating the slope of the force-displacement curves in the initial linear region. A good agreement can be observed with experimental and numerical results. However, the differences between the experimental and

numerical results may be for different reasons, such as: (a) the mechanical properties which defined for the behavior of the material in the finite element simulations, were based on the results of the tensile tests of the dumbbell-shaped specimens. This is while the printing orientation of the layers in the dumbbell sample is considered to be $\pm 45^\circ$ to provide an appropriate approximation, although the printing orientation of different structures is not consistent and is not accurately equal to $\pm 45^\circ$. (b) Considering the layer-by-layer production process in the FDM method, it should be noted that the specimens manufactured by this method have a certain degree of anisotropy[6] that is not considered in FEM simulation. (c) The thickness defined for the cell wall in the finite element simulation was exactly one millimeter, while the thickness of the specimens produced by 3D printing had about 5% dimensional tolerance. (d) The mechanical properties of 3D Printed ABS polymers may change slightly when exposed to different environmental air conditions with variable humidity and temperatures. Since the printing and testing of tensile and flexural test specimens has been performed at different times, this may affect their properties which make difference between the experimental and finite element results.

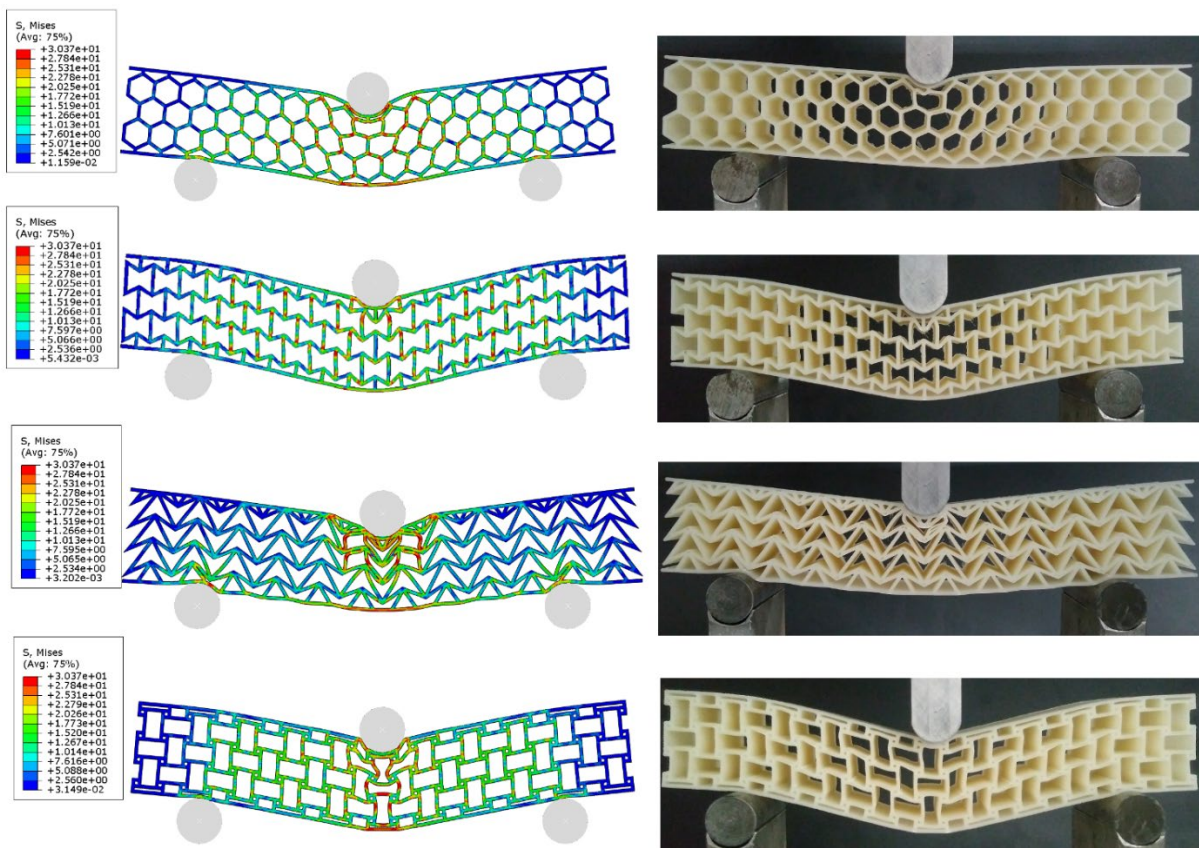


Fig. 10. Comparison of experimental and numerical deformation patterns and failure modes of beams

(e) Notably, another reason for the difference between experimental and numerical results, related to delamination of some printed layers during three point bending tests which is related to the manufacturing process (see Fig. 11). Moreover, as shown in Fig. 12 during three point bending tests in some specimens, the fracture of walls of the unit cells was occurred which is not considered in the finite element simulation.

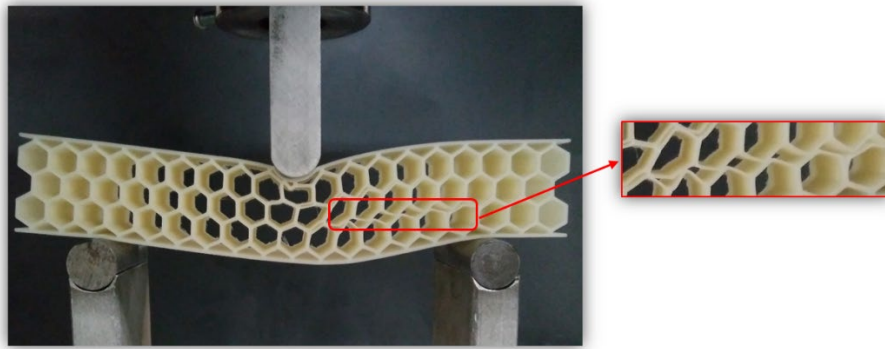


Fig. 11. Delamination of 3D printed layers under three point bending tests is some of the unit cells

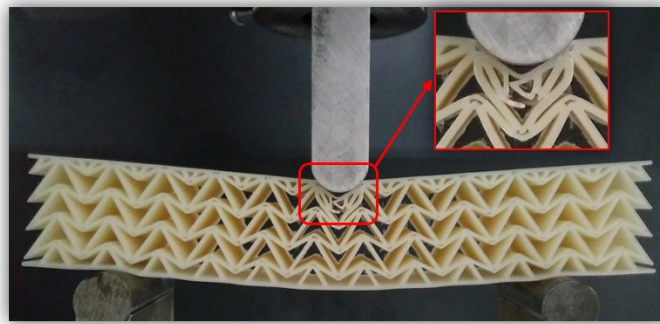


Fig. 12. Failure of cell wall of the unit cell that causes a slight sudden drop on the load displacement curve.

Table 5. Experimental and numerical comparison of maximum load and flexural stiffness of sandwich beams with different core topologies

Structure	Flexural stiffness (N/mm)		Maximum Load (N)	
	Exp	FEA	Exp	FEA
Honeycomb	119.153	134.02	472	697.551
Re-entrant	89.799	55.989	645.6	492.736
Arrowhead	240.067	256.06	1023.2	951.83
Square node Anti-tetra chiral	81.618	87.664	758.4	769.275

The experimental load-displacement curves for one specimen of different 3D printed sandwich beams are shown in Fig. 13. All the structures are composed of 19×4 unit cells with span to thickness ratio of 4 and equal depth and thickness. Experimental results show that the core geometry of the sandwich beams has a significant impact on the performance of these structures.

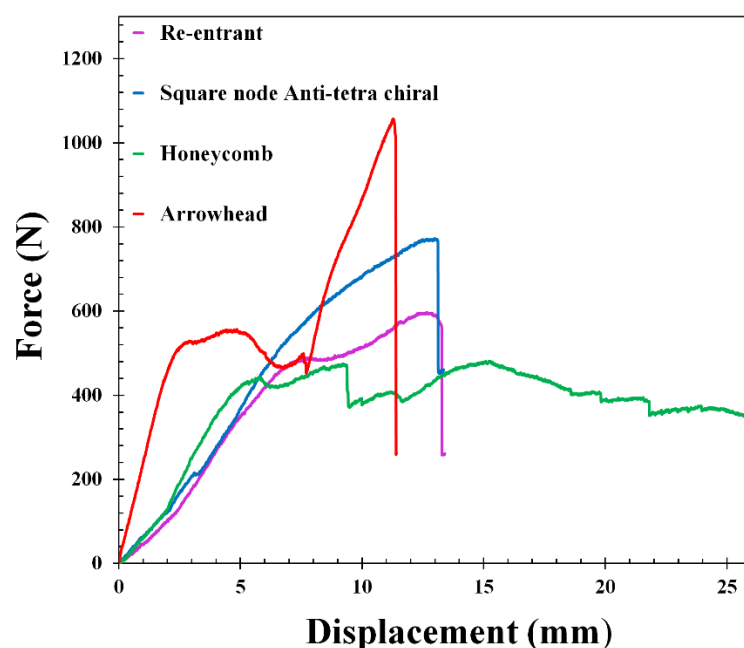


Fig. 13. Experimental load-displacement curves of 3D printed sandwich beams obtained by three point bending tests

Fig. 14 presents and compares experimental results for maximum load, displacement at failure, flexural stiffness and specific energy absorption of sandwich beams with four different core topologies. The specific energy absorption is obtained by dividing the amount of energy absorbed by the weight of the structures. It should be noted that the energy absorption of the sandwich beam structures is obtained by calculating the area under the force-displacement curve up to displacement which failure is occurred. Accordingly, the highest amount of specific energy absorption is related to the honeycomb sandwich beam, due to its high deflection at failure, compared to auxetic sandwich beams (see Fig. 13). Whereas, if the identical amount of displacement, such as 10 mm is considered for calculating the energy absorption of beams, all the sandwich beams with auxetic core, behave better than honeycombs sandwich core in the energy absorption capability.

On average, compared to non-auxetic honeycomb sandwich beam, the auxetic core beams improved load bearing capacity of sandwich beams, while decreasing their flexural stiffness. Only arrowhead sandwich beam had higher flexural stiffness than honeycomb beam, whereas the load bearing capacity of all the auxetic beams was higher than honeycomb beam.

The auxetic arrowhead sandwich beam had the maximum load bearing capacity, maximum flexural stiffness and minimum specific energy absorption. Moreover, the minimum flexural stiffness was related to square node anti-tetra chiral auxetic beam. Auxetic arrowhead with a maximum load of (1023.2 N) and non-auxetic honeycomb with (472 N) beams had the highest and the lowest load bearing capacity among four sandwich beams. Furthermore, the highest deflection was related to honeycomb beam structure with 25.889 mm displacement at failure.

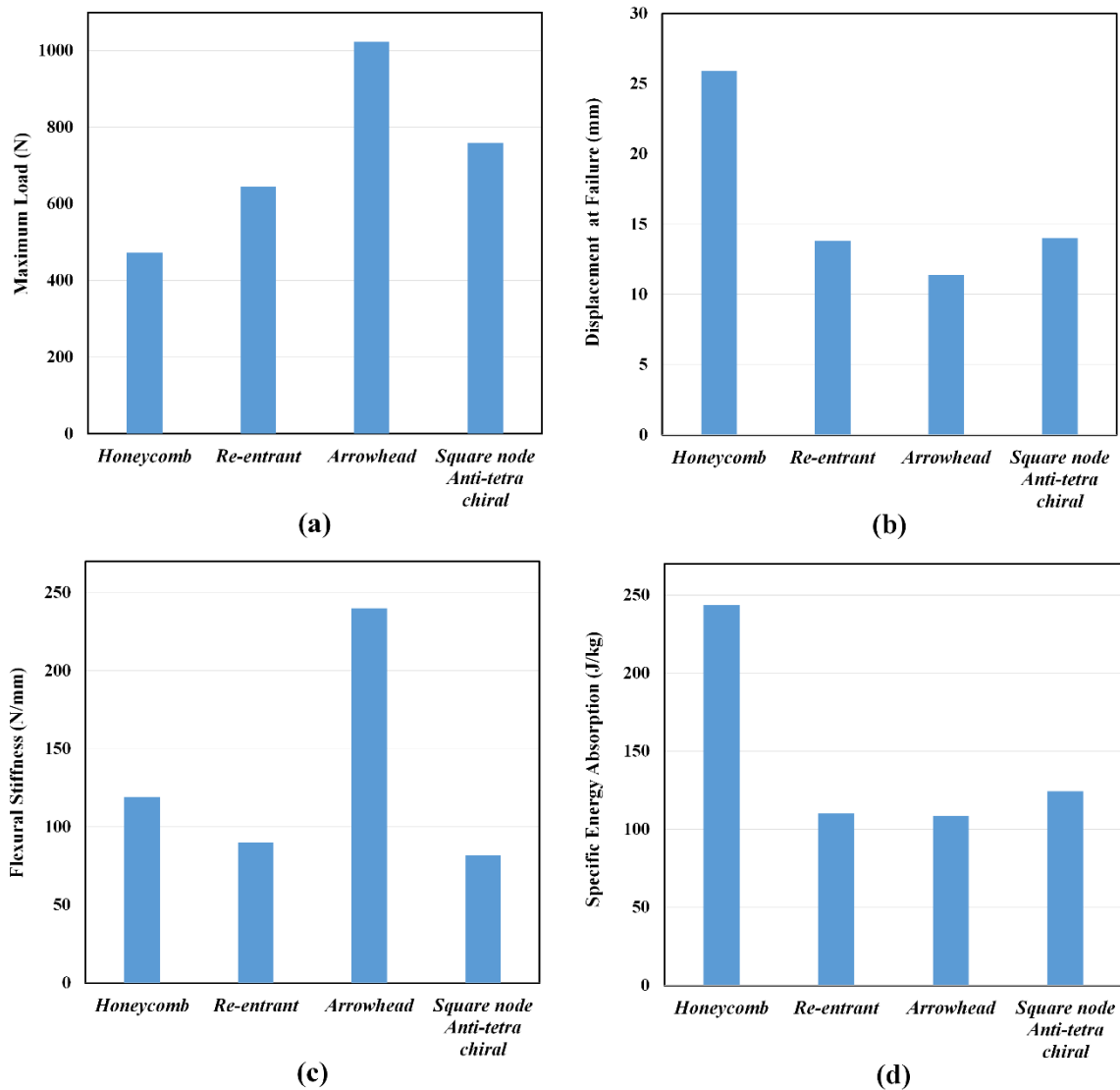


Fig. 14. Bending properties of 3d printed sandwich beams obtained by three-point bending tests: (a) maximum load, (b) displacement at failure, (c) flexural stiffness and (d) specific energy absorption

4. Conclusions

The aim of this work was to study the effect of using auxetic cores on the flexural properties of sandwich beams. Hence, three types of auxetic cores, including square node anti-tetra chiral,

arrowhead and re-entrant are used to create sandwich beams. Moreover, a non-auxetic honeycomb core sandwich beam was assessed and compared with auxetic core sandwich beams. Numerical and experimental approaches were implemented to evaluate the flexural behavior of beams. A total number of 12 specimens were manufactured using FDM 3D printing method and tested under three point bending. The load-deflection behavior, energy absorption, stiffness and load bearing capacity of the specimens were evaluated. A finite element analysis was also carried out to compute mechanical properties of beams and compare with experimental results. Results demonstrated that the cellular design of the core topology has significant influence on the failure mode and the energy absorption of the sandwich beams. As an example, beams with auxetic core, have good energy absorption capability (108.3.17-124.247 J/kg), however, in this respect, the honeycomb core sandwich beam (243.64 J/kg) exhibit better performance duo to its higher deflection compared with its counterparts made of auxetic core designs. Using of auxetic cores significantly increased the load bearing capacity of sandwich beams and the beam with arrowhead core which had the highest load bearing capacity, could afford 116.8% load higher than honeycomb core sandwich beam. This study on four different sandwich beams indicated that, in order to selection of core topology to use in sandwich beams, various properties such as stiffness, load bearing capacity and specific energy absorption should be considered and according to the intended application, the desirable beam should be used.

Funding

This work was supported by Iran National Science Foundation (INSF) through grant program No. 98008972.

References

- [1] J. Ju, J.D. Summers, Compliant hexagonal periodic lattice structures having both high shear strength and high shear strain, *Mater. Des.* 32 (2011) 512–524. <https://doi.org/https://doi.org/10.1016/j.matdes.2010.08.029>.
- [2] N.S. Ha, G. Lu, X. Xiang, Energy absorption of a bio-inspired honeycomb sandwich panel, *J. Mater. Sci.* (2018). <https://doi.org/10.1007/s10853-018-3163-x>.
- [3] V. Daliri, A. Zeinedini, Flexural Behaviour of the Composite Sandwich Panels with Novel and Regular Corrugated Cores, (2019) 963–982.
- [4] M. Spahic, N. Di Cesare, A. Le Duigou, V. Keryvin, Multi-scale analysis of the flexural behaviour of 3D printed cellular polymer materials: Comparison between morphing and sandwich beams, *Compos. Struct.* 273 (2021) 114249. <https://doi.org/https://doi.org/10.1016/j.compstruct.2021.114249>.
- [5] T.A. Schaedler, W.B. Carter, Architected Cellular Materials, *Annu. Rev. Mater. Res.* 46 (2016) 187–210. <https://doi.org/10.1146/annurev-matsci-070115-031624>.
- [6] H.Y. Sarvestani, A.H. Akbarzadeh, A. Mirbolghasemi, K. Hermenean, 3D printed meta-sandwich structures : Failure mechanism , energy absorption and multi-hit capability Face-sheets, *Mater. Des.* 160 (2018) 179–193. <https://doi.org/10.1016/j.matdes.2018.08.061>.
- [7] W. Ahmed, S. Ahmed, F. Alnajjar, E. Zaneldin, Mechanical performance of three-dimensional printed sandwich composite with a high-flexible core, *Proc. Inst. Mech. Eng. Part L J. Mater. Des. Appl.* 235 (2021) 1382–1400. <https://doi.org/10.1177/14644207211011729>.
- [8] S.Z. Gebrehiwot, L. Espinosa Leal, J.N. Eickhoff, L. Rechenberg, The influence of stiffener geometry on flexural properties of 3D printed polylactic acid (PLA) beams, *Prog. Addit. Manuf.* 6 (2021) 71–81. <https://doi.org/10.1007/s40964-020-00146-2>.
- [9] B.D. de Castro, F. de C. Magalhães, T.H. Panzera, J.C. Campos Rubio, An Assessment of Fully Integrated Polymer Sandwich Structures Designed by Additive Manufacturing, *J. Mater. Eng. Perform.* (2021). <https://doi.org/10.1007/s11665-021-05604-8>.
- [10] S.M. Zaharia, L.A. Enescu, M.A. Pop, Mechanical Performances of Lightweight Sandwich Structures Produced by Material Extrusion-Based Additive Manufacturing, *Polym.* . 12 (2020). <https://doi.org/10.3390/polym12081740>.
- [11] X. Ren, R. Das, P. Tran, T.D. Ngo, Y.M. Xie, Auxetic metamaterials and structures: a review, *Smart Mater. Struct.* 27 (2018) 023001. <https://doi.org/10.1088/1361-665X/aaa61c>.
- [12] X. Ren, J. Shen, A. Ghaedizadeh, H. Tian, Y. Min Xie, Experiments and parametric studies on 3D metallic auxetic metamaterials with tuneable mechanical properties, *Smart Mater. Struct.* 24 (2015) 95016. <https://doi.org/10.1088/0964-1726/24/9/095016>.
- [13] Q. Gao, C. Ge, W. Zhuang, L. Wang, Z. Ma, Crashworthiness analysis of double-arrowed auxetic structure under axial impact loading, *Mater. Des.* 161 (2019) 22–34. <https://doi.org/10.1016/j.matdes.2018.11.013>.
- [14] W. Wu, Y. Tao, Y. Xia, J. Chen, H. Lei, L. Sun, Mechanical properties of hierarchical anti-tetrachiral metastructures, *Extrem. Mech. Lett.* 16 (2017) 18–32. <https://doi.org/10.1016/j.eml.2017.08.004>.
- [15] T.-C. Lim, Introduction BT - Auxetic Materials and Structures, in: T.-C. Lim (Ed.), Springer Singapore, Singapore, 2015: pp. 1–43. https://doi.org/10.1007/978-981-287-275-3_1.
- [16] M.S. Mazloomi, M. Ranjbar, Hybrid Design Optimization of Sandwich Panels with Gradient Shape Anti-

- Tetrachiral Auxetic Core for Vibroacoustic Applications, *Transp. Porous Media.* (2021).
<https://doi.org/10.1007/s11242-021-01646-7>.
- [17] A. Hosseinkhani, D. Younesian, M. Ranjbar, F. Scarpa, Enhancement of the vibro-acoustic performance of anti-tetra-chiral auxetic sandwich panels using topologically optimized local resonators, *Appl. Acoust.* 177 (2021) 107930. <https://doi.org/https://doi.org/10.1016/j.apacoust.2021.107930>.
- [18] A. Hosseinkhani, D. Younesian, M. Ranjbar, Vibro-Acoustic Analysis and Topology Optimization of Anti-Tetra Chiral Auxetic Lattices Driven by Different Colored Noises, *Int. J. Struct. Stab. Dyn.* 20 (2020) 2050113. <https://doi.org/10.1142/S0219455420501138>.
- [19] A. Alomarah, S.H. Masood, I. Sbarski, B. Faisal, Z. Gao, Compressive properties of 3D printed auxetic structures : experimental and numerical studies, *Virtual Phys. Prototyp.* 2759 (2019). <https://doi.org/10.1080/17452759.2019.1644184>.
- [20] M. Najafi, H. Ahmadi, G. Liaghat, Experimental investigation on energy absorption of auxetic structures, *Mater. Today Proc.* 34 (2021) 350–355. <https://doi.org/https://doi.org/10.1016/j.matpr.2020.06.075>.
- [21] H. Huang, B. Wong, Y. Chou, I. Poisson, N. Poisson, Design and properties of 3D-printed chiral auxetic metamaterials by reconfigurable connections, 8 (2016) 1–8. <https://doi.org/10.1002/pssb.201600027>.
- [22] A. Ingrole, A. Hao, R. Liang, Design and modeling of auxetic and hybrid honeycomb structures for in-plane property enhancement, *Mater. Des.* 117 (2017) 72–83. <https://doi.org/10.1016/J.MATDES.2016.12.067>.
- [23] C. Qi, A. Remennikov, L.-Z. Pei, S. Yang, Z.-H. Yu, T.D. Ngo, Impact and close-in blast response of auxetic honeycomb-cored sandwich panels: Experimental tests and numerical simulations, *Compos. Struct.* 180 (2017) 161–178. <https://doi.org/10.1016/J.COMPSTRUCT.2017.08.020>.
- [24] M. Safikhani Nasim, E. Etemadi, Three dimensional modeling of warp and woof periodic auxetic cellular structure, *Int. J. Mech. Sci.* 136 (2018) 475–481. <https://doi.org/https://doi.org/10.1016/j.ijmecsci.2018.01.002>.
- [25] B. Šubic, G. Fajdiga, J. Lopatič, Bending Stiffness, Load-Bearing Capacity and Flexural Rigidity of Slender Hybrid Wood-Based Beams, *Forests.* 9 (2018) 703. <https://doi.org/10.3390/f9110703>.
- [26] S. Hou, T. Li, Z. Jia, L. Wang, Mechanical properties of sandwich composites with 3d-printed auxetic and non-auxetic lattice cores under low velocity impact, *Mater. Des.* 160 (2018) 1305–1321. <https://doi.org/https://doi.org/10.1016/j.matdes.2018.11.002>.
- [27] P. Sadeghian, D. Hristozov, L. Wroblewski, Experimental and analytical behavior of sandwich composite beams: Comparison of natural and synthetic materials, *J. Sandw. Struct. Mater.* 20 (2016) 287–307. <https://doi.org/10.1177/1099636216649891>.
- [28] L.J. Gibson, M.F. Ashby, *Cellular Solids: Structure and Properties*, 2nd ed., Cambridge University Press, Cambridge, 1997. [https://doi.org/DOI: 10.1017/CBO9781139878326](https://doi.org/DOI:10.1017/CBO9781139878326).